Response surface methodology for optimization of photocatalytic degradation of aqueous ammonia

Rania Farouq, M. Abd-Elfatah and M. E. Ossman

ABSTRACT

Ammonia removal from synthetic wastewater was studied through a photocatalytic degradation process under UV light. In this study, TiO_2/C_3N_4 was synthesized through a simple method of preparing g-C_3N_4 through the pyrolysis of melamine then adding it to TiO_2. On the other hand, ZnO/C_3N_4 composite was prepared by a deposition–precipitation technique. The composites were described by Fourier transform infrared spectroscopy (FTIR), X-ray powder diffraction (XRD) and scanning electron microscope (SEM). Response surface methodology (RSM) has been utilized to model variables using Minitab 18. Calculated values of degradation efficiency were in good agreement with experimental values ($R^2 = 0.97$ and Adj–$R^2 = 0.91$). The influence of parameters over ammonia initial concentration (10–50 ppm), catalyst dosage (0.2–1.5 g), light intensity (6–30 W) and stirring speed (100–500 rpm) on ammonia removal percentage was investigated, and their main and interaction contribution was examined. The optimum conditions of the degradation were observed at a dosage of 1 g/L and initial concentration of ammonia 10 ppm for UV intensity irradiation with 24 W lamps. It was concluded that the photocatalytic degradation of the ammonia solution, after 50 min of UV irradiation, can reach percentages of 46%, and 52% using the catalysts TiO_2/g-C_3N_4 and ZnO/g-C_3N_4, respectively.

Key words | ammonia removal, C_3N_4, photocatalyst, RSM, TiO_2, UV light, ZnO

Rania Farouq (corresponding author)
M. Abd-Elfatah
M. E. Ossman
Petrochemical Engineering Department,
Pharos University,
Alexandria,
Egypt
E-mail: *rania.farouq@pua.edu.eg*

M. E. Ossman
Informatic Research Institute (IRI), City for Scientific Research and Technology Applications (CSAT),
Borg Elarab, Alexandria,
Egypt

INTRODUCTION

Ammonia is a major aquatic pollutant which accelerates the eutrophication and causes an increase of oxygen demand. The permitted level of ammonia is beneath 1 ppm (Luo *et al.* 2015). It was concluded that when ammonia was released in water sources, fish could experience ammonia poisoning (Gupta *et al.* 2015).

The photocatalytic oxidation of NH_3 is viewed as a promising approach to detoxify animal waste containing effluents by a singular walk handle. The fundamental examinations go back to the 1980s, when the photodecomposition of vaporous ammonia on ultraviolet (UV) illuminated anatase TiO_2 particles was first considered by Mozzanega *et al.* (Altomare *et al.* 2014). The illumination of a semiconductor photocatalyst with UV radiation activates the catalyst, establishing a redox environment in the aqueous solution. TiO_2 can be activated using UV illumination with a wavelength up to 387.5 nm. In the meantime, solar irradiation starts at a wavelength of about 300 nm. However, the content of UV in sunlight is only 3–4%. Consequently, it limits the use of sunlight as an energy source (Dong *et al.* 2012).

TiO_2 was utilized to break N-H bonds and study the instrument of NH_3 deterioration (Zhou *et al.* 2016). A few studies have demonstrated that the photocatalytic method can destroy N-H bonds (Shavisi *et al.* 2013; Altomare *et al.* 2014).

doi: 10.2166/aqua.2018.121

Some investigations demonstrated that TiO_2 addresses the most promising photocatalyst for such a response, since the oxidizing species productively photograph delivered on its surface can oxidize NH_3, generally into nitrite and nitrate particles (Mikami *et al.* 2010), which, however, are also noxious. Consequently, the most alluring approach to completely remove nitrogen-containing wastes is the selective photocatalytic oxidation of NH_3 into innocuous N_2. Therefore, the mechanism of NH_3 photocatalytic oxidation has to be examined by taking into account the distribution of the final reaction products (Mikami *et al.* 2010). Recently, some of the researchers methodically investigated the impact different experimental conditions have on the photocatalytic abatement of NH_3 in aqueous suspensions and on the selectivity toward its oxidation products (Altomare *et al.* 2014).The deposition of metal nanoparticles on TiO_2 was investigated, focusing on the impacts of the type/amount of metal on the reaction pathways and product selectivity, even by coupling ammonia abatement with hydrogen production (Yuzawa *et al.* 2012) or with NO reduction. The response has been researched using both TiO_2 and different semiconductor materials as photocatalysts (Shavisi *et al.* 2013), also with the trial of tailoring them toward NH_3 selective conversion into innocuous N_2 (Mikami *et al.* 2010; Altomare *et al.* 2014).

Among the utilized photocatalysts, ZnO has demonstrated a high capability in photocatalytic degradation as a result of its remarkable band crevice vitality and ease (Xiong *et al.* 2009). Zinc oxide (ZnO) is an important photocatalyst due to its similar band gap energy and required band gap sites compared with titanium dioxide (TiO_2). The main factor affecting the photocatalytic activity of ZnO is the quick recombination of charge carriers. In order to improve the photocatalytic activity; ZnO was doped by metals and metal oxides (Achouri *et al.* 2014); these doping composites broaden the absorption spectrum of this semiconductor toward the visible-light region, as new energy levels are formed between its valence and conduction bands (Xiong *et al.* 2009).

Graphitic carbon nitride (g-C_3N_4) has high activity for the photodegradation of pollutants in waste water with the benefits of high thermal and chemical stability. Graphitic carbon nitride (g-C_3N_4) is investigated as a sensitizer candidate possessing several advantages towards other photocatalysts; and shows a clear decrease in band gap values for g-C_3N_4 TiO_2 systems (Li *et al.* 2009; Miranda *et al.* 2013).

For these reasons, the combination of ZnO or TiO_2 with C_3N_4 may be an excellent photocatalyst to achieve an enhanced charge separation in electron-transfer processes. Our research on TiO_2 coupled with g-C_3N_4, and ZnO coupled with g-C_3N_4 were carried out to upgrade the photocatalytic activity for the ammonia degradation in water samples that simulated those from the effluent from the fertilizer industry.

In this study, we used the response surface methodology (RSM) for the experimental condition optimization. The use of factorial designs leads to optimized parameters with a minimum set of runs and also to the possibility of obtaining a polynomial expression that describes the process yield (Bali 2004; Oliveira *et al.* 2006).

MATERIALS AND METHODS

Melamine, titanium dioxide, zinc chloride, sodium carbonate, zinc nitrate, sodium hydroxide and soluble starch were utilized as precursors for the synthesis of photocatalysts composites. All chemicals were utilized as acquired without further purification.

Synthesis of g-C_3N_4

The g-C_3N_4 photocatalyst was incorporated by heating melamine powder. Five grams of melamine powder was placed into an alumina pot crucible heated in a muffle furnace at 520 °C for 4 h, g-C_3N_4 was obtained.

TiO_2 coupled with g-C_3N_4 photocatalyst preparation

Graphitic carbon nitride–-TiO_2 composites were accomplished by a simple impregnation method. In a typical technique, 0.25 g of g-C_3N_4 and 10 g of TiO_2 were dissolved into methanol and sonicated independently for 30 min. At that point the two slurries were blended and stirred at room temperature for 24 h. Later, the composite photocatalysts were acquired by evaporating the methanol in a rotary evaporator at 80 °C.

ZnO coupled with g-C_3N_4 photocatalyst preparation

The precursors of C_3N_4/ZnO photocatalysts were submitted to a deposition–precipitation technique at room temperature, in which 0.074 g of melamine was dissolved in 25 mL of $ZnCl_2$ (0.5 mol/L) solution in a 250 mL beaker, and the suspension was mixed for 20 min. At that point, 25 mL of Na_2CO_3 (0.5 mol/L) solution was added drop wise into the above suspension and stirred magnetically for 30 min. Subsequently, the mixture was filtered, washed with deionized water many times, and dried at 60 °C for 24 h. The precursor of C_3N_4/ZnO photocatalyst in the C_3N_4 ratio of 5.0 wt.% was obtained.

Characterization

The surface functional groups and structure were investigated by Fourier transform infrared (FTIR) spectroscopy. The FTIR spectra of the TiO_2-C_3N_4 and ZnO-C_3N_4 mixtures were recorded between 500 and 4,000 cm^{-1}.

The X-ray diffraction (XRD) patterns of the samples were measured to confirm the prepared composite formations.

A scanning electron microscope (SEM) was employed to visualize sample morphology. In the present study, the samples prepared were analyzed by using SEM JEOL JSM 6,360 L and were taken at 20,000 and 35,000 magnification.

Photocatalytic experiment

The glass reactor (inner volume: 2 L) was utilized for the photodegradation of ammonia from synthetic waste water samples. The system was illuminated with a 12 W lamp with a peak light intensity at 365 nm, covering the glass reactor. The initial pH was measured and adjusted to the desired value (pH = 10 using HCl and/or NaOH solution), this is because the number of OH^- ions increases when pH increases, and more OH ions generated result in promoting the degradation rate of ammonia nitrogen. Also, there are two forms of ammonia nitrogen present in water: NH_3 and NH^{4+}. The ratio of NH_3 molecules increases when the pH increases in the solution (Luo *et al.* 2015). The entire system was protected by a black case during the reaction to obstruct outside light. Catalyst granules were stirred in 2.0 L of ammonia waste water solutions and exposed to the UV source. The temperature of the suspension was kept at 20 ± 8 °C, and the irradiation time was 50 min. A needle-type probe was inserted in the reactor to withdraw samples. The liquid sample (<5.0 mL) was collected in a vial wrapped in aluminum foil to reduce interference from indoor fluorescent light before the analysis. The concentration of residual ammonia was determined by simple titration against sulphoric acid.

Central composite design

Central composite design (CCD) was utilized for optimization of four factors (initial ammonia concentration, irradiation intensity, stirring speed and catalyst dosage) to gather information about their impact. The number of conducted experiments was calculated as follows:

$$N = 2^k + 2k + n_c \quad (1)$$

where k is the number of variables and n_c is the number of central points. The coded levels and the natural values of variables shown in Table 1 were initial ammonia concentration (X_1), catalyst dosage (g/L) (X_2), irradiation intensity (Watt) (X_3) and stirring speed (rpm) (X_4) that were coded as X_i according to the following equation:

$$x_i = \frac{X_i - X_o}{\Delta X} \quad (2)$$

where X_o is the value of X_i at the central point, and ΔX_i is the step change.

The removal percentage dependency to all variables can be represented as follows:

$$y = \beta_0 + \sum_{i=1}^{k} \beta_i X_i + \sum_{i=1}^{k-1} \beta_{ii} X_i^2 + \sum_{i=1}^{k-1} \sum_{j=1}^{k} \beta_{ij} X_i X_j + \varepsilon \quad (3)$$

Table 1 | Design matrix for the central composite designs

Factors	Low (−1)	Central (0)	High (+1)	$-\alpha$	$+\alpha$
Initial concentration ppm	20	30	40	10	50
Dosage (g)	0.2	0.5	0.8	0.1	1
Light intensity	12	18	24	6	30
Stirring speed (rpm)	200	300	400	100	500

where y is the response, β_0, β_i, β_{ii} are the regression coefficients of variables for intercept, linear, quadratic and interaction terms, respectively. X_i and X_j are the independent variables and ε is the residual term. The Minitab software (version 18) was used for data processing. The analysis of variance (ANOVA) was performed to justify the significance and adequacy of the developed regression model according to the determination coefficient (R^2).

RESULTS AND DISCUSSION

Characterization of photo catalyst

FTIR analysis

The FTIR spectra of composites are shown in Figures 1 and 2. For the TiO_2-C_3N_4 mixture, a few peaks relating to TiO_2 are noticed. The broad band centered at 500–600 cm^{-1} is likely due to the vibration of the Ti–O bonds in the TiO_2 lattice and the peaks in the 500–1,000 cm^{-1} region are allotted to the vibrations of the Ti–O and Ti–O–Ti framework bonds (Komatsu 2001a). Some strong bands in the 1,242–1,639 cm^{-1} area are the stretching modes of CN heterocyclic (Komatsu 2001a, 2001b, 2001c). The two absorption peaks at 1,300–1,412 and 1,529–1,639 cm^{-1} are appointed, individually, to C(sp2)–N (1,325 cm^{-1}) and C(sp2) = N (1,639 cm^{-1}) stretching modes in a graphite-type structure; such a band is not allowed in the FTIR spectrum of pure graphite single crystals. The broad peaks allocated at 3,100–3,600 cm^{-1} are assigned to vibrations of hydroxyl groups (Salavati-Niasari *et al.* 2011).

For the ZnO-C_3N_4 mixture, Figure 2 demonstrates that the peak at 1,632.2 cm^{-1} is related to Zn–O stretching, while the peak noticed at 3,446.3 cm^{-1} may be because of O–H stretching assigned to the water adsorption on the metal surface. The sharp peak positioned at 471.6 cm^{-1} is attributed to the Zn–O stretching bonds. The IR bands in the region of 1,700–600 cm^{-1} correspond to C = O, C–O and C–H vibrations respectively (Xiong *et al.* 2009). Several strong bands in the 1,242–1,639 cm^{-1} region are the stretching modes of CN heterocyclic (Komatsu 2001a, 2001b, 2001c). The two absorption peaks at 1,300–1,412 cm^{-1} and 1,529–1,639 cm^{-1} are allocated, respectively, to C(sp2)–N (1,387 cm^{-1}) and C(sp2) = N (1,632 cm^{-1}) stretching modes in a graphite-type structure (such a band is forbidden in the FTIR spectrum of pure graphite single crystals). The broad peaks appearing at 3,100–3,600 cm^{-1} are assigned to vibrations of hydroxyl groups (Salavati-Niasari *et al.* 2011).

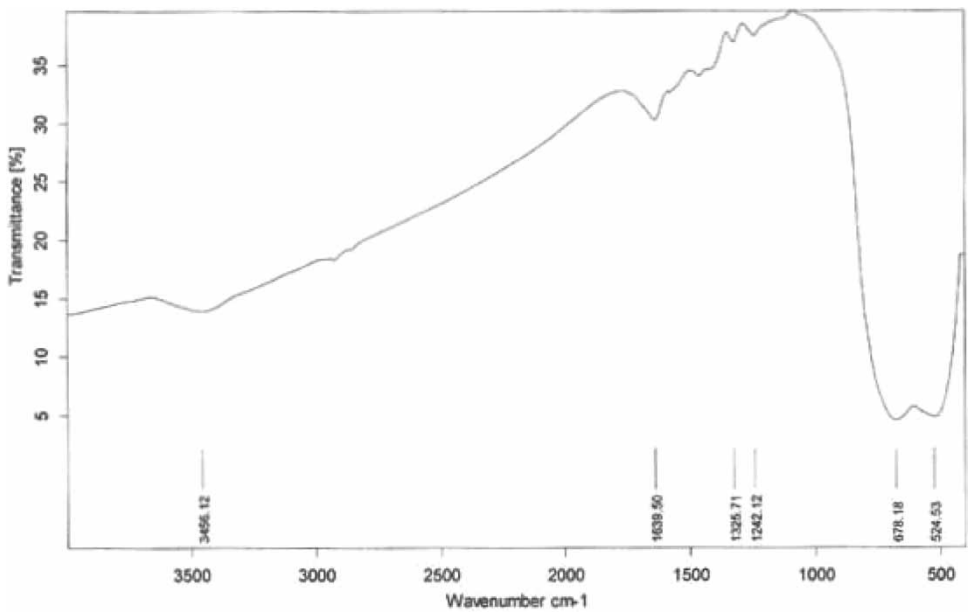

Figure 1 | FTIR analysis of TiO_2-C_3N_4.

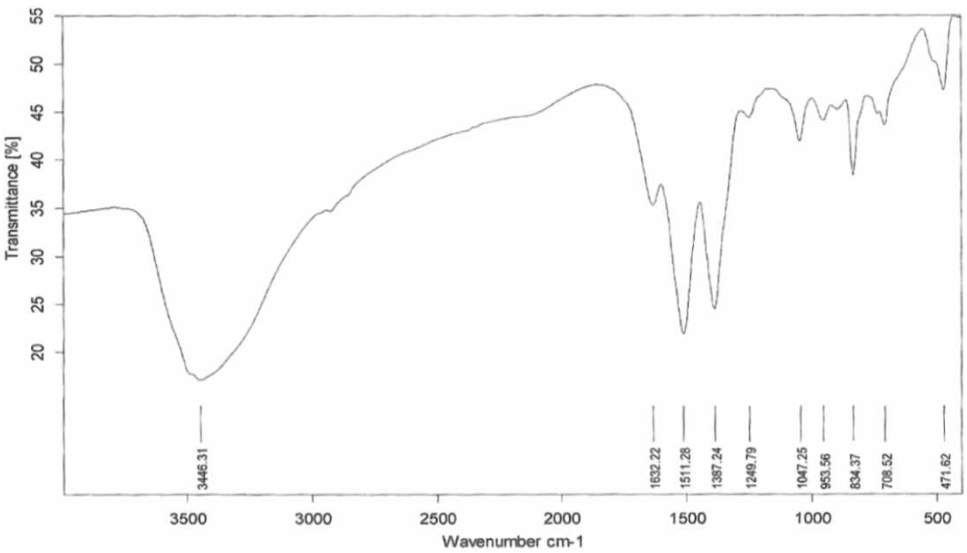

Figure 2 | FTIR analysis of ZnO-C_3N_4.

SEM analysis

The surface morphology of TiO_2-C_3N_4 and ZnO-C_3N_4 are shown in Figures 3 and 4. Figure 3 shows that the sample of TiO_2-C_3N_4 appeared to have aggregated particles that contained many smaller crystals and well-crystallized C_3N_4 nanostructures that the TiO_2 aggregates covering the C_3N_4 particles.

Figure 4 shows the sample of ZnO-C_3N_4. It is clearly seen that the ZnO-C_3N_4 composite appears to be spherical in shape with a smooth surface like agglomerate, which is composed of many small spherical nanoparticles which may be because the melamine plays a conglomeration role in the chemical precipitation process. It can be inferred that ZnO is uniformly distributed on the surface of the sphere-like composite, which favors the formation of heterojunction and results in an increase in the specific surface areas, which is beneficial to the photocatalytic activity. Particle size also plays a critical role in the photocatalytic activity which was found to increase with increasing particle size for spherical diameters smaller than 200 nm (Amano *et al.* 2013).

XRD analysis

Figures 5 and 6 show the XRD for TiO_2-C_3N_4 and ZnO-C_3N_4 mixtures. For TiO_2-C_3N_4 composite, it can be seen

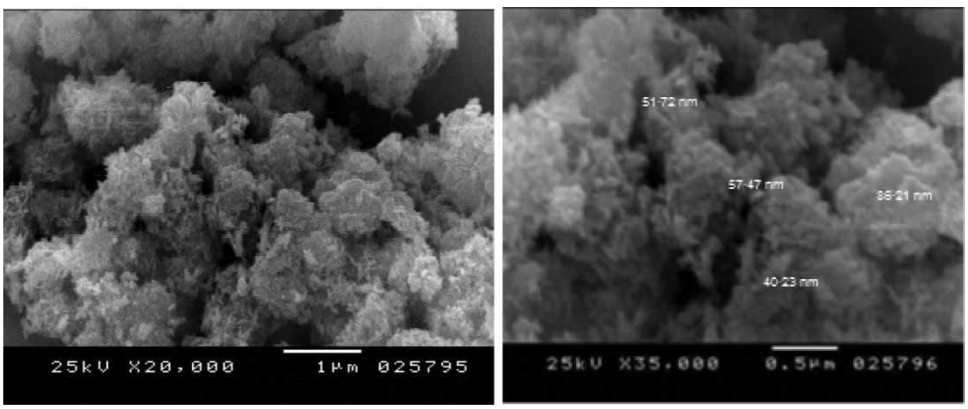

Figure 3 | SEM analysis of TiO_2-C_3N_4 with different magnification factor.

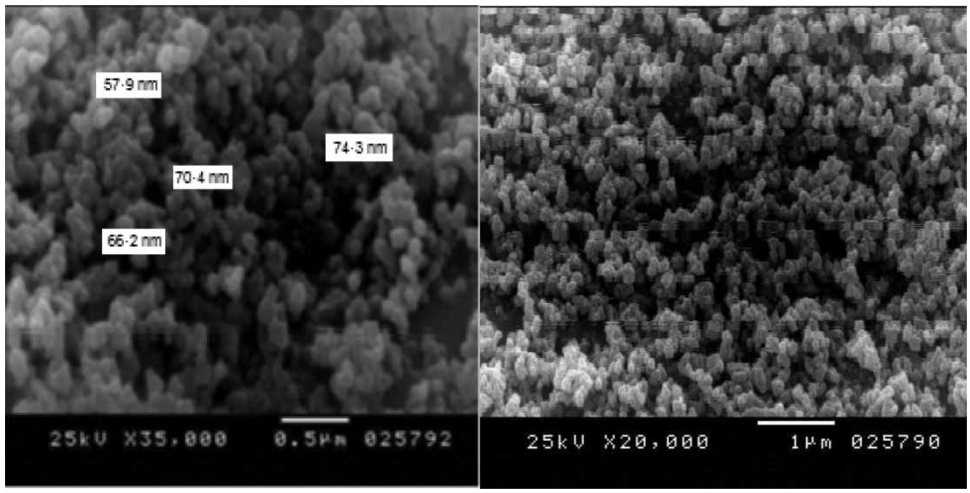

Figure 4 | SEM analysis of ZnO-C_3N_4 with different magnification factor.

from Figure 5 that the peaks appeared at 2θ values, the diffraction peak at 2θ with 25.3, 38.3, 48, 54, 62, 74, 76 and 83° corresponds to the crystal planes of (101), (004), (200), (105), (204), (213), (107), (301) indicating the formation of anatase phase of TiO_2. The peaks of the graph are in good agreement with the literature (Akarsu *et al.* 2006; Jiang *et al.* 2011). The location of the peaks was contrasted to values in literature and the existence of titanium dioxide particles was affirmed. Also, the figure shows that a strong peak at 2θ value with 26° corresponds to the crystal planes of (110), indicating the formation of α-C_3N_4.

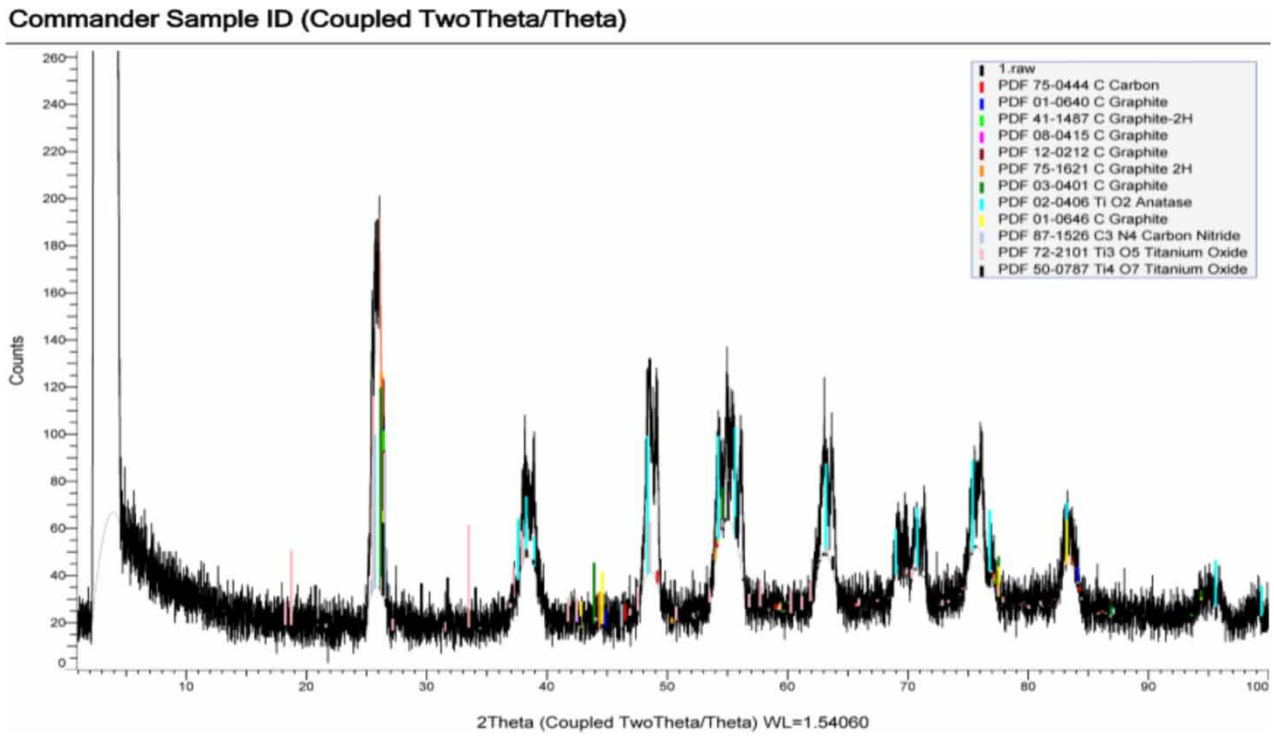

Figure 5 | XRD analysis of TiO_2-C_3N_4.

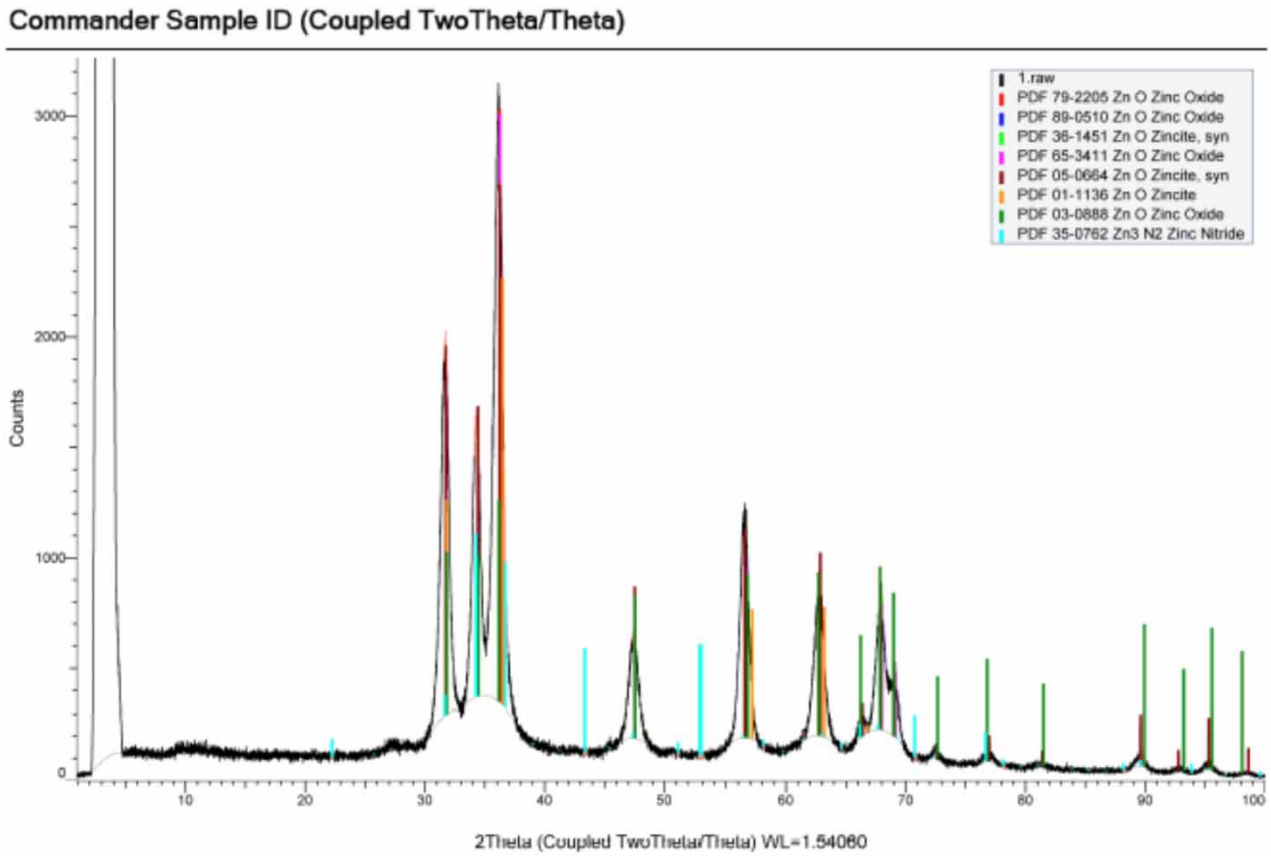

Figure 6 | XRD analysis of ZnO-C_3N_4.

For ZnO-C_3N_4 composite, it can be seen from Figure 6 that the peaks appeared at 2θ values, the diffraction peak at 2θ with 31.74, 36.83, 47.62, 56.7, 62.7, and 68° are observed corresponding to (100), (101), (102), (110), (103), and (112) crystal planes indicating the formation of ZnO, the peaks of the graph are in good agreement with the literature (Alwan *et al.* 2015). Also, all peaks are indexed according to the hexagonal phase of ZnO. There are strong peaks at 2θ values, the diffraction peak at 2θ with 32, 34, and 36° appeared to correspond with (321) crystal planes indicating the formation of Zn_3N_2 (Jiangyan *et al.* 2012).

Experimental design and optimization

The impact of four variables on ammonia removal from aqueous solutions was researched by conduction of a total of 31 runs (see Table 2); their results were analyzed by ANOVA to obtain an empirical equation that can predict the real behavior of the adsorption system.

Analyses of experimental results gave the following empirical relationship:

$$\begin{aligned} y = {} & 26.283 - 15.490^{*}X_1 + 40.281^{*}X_2 - 24.945^{*}X_3 \\ & + 17.774^{*}X_4 + 2.853^{*}X_1^2 - 8.308^{*}X_2^2 - 28.881^{*}X_3^2 \\ & + 6.121^{*}X_4^2 - 1.831^{*}X_1{}^{*}X_2 - 19.216X_1{}^{*}X_3 \\ & + 61.389^{*}X_2{}^{*}X_3 + 32.9^{*}X_3{}^{*}X_4 \end{aligned} \quad (4)$$

The determination coefficient and residuals of the ANOVA in Table 3 were used to check the statistical adequacy of the model; in which the F test indicates the relationship between the mean square and the residual error of the model.

The fitness of the model was also indicated by its high R^2 value (0. 967) and adjusted R^2 value of 0.946. According to a

Table 2 | The experimental design with variables response

Run no.	Initial concentration (ppm)	Dosage (g)	Light intensity	Stirring speed (rpm)	% Removal (observed)	% Removal (predicted)
1	10	1	12	300	44.3	42.46
2	20	1	12	300	36.4	37.17
3	30	1	18	300	35.1359	35.14
4	40	1	12	300	30.1	30.87
5	50	1	12	300	28.6	29.85
6	10	0.2	12	300	20.3	20.54
7	10	0.5	6	300	29.4451	29.45
8	10	0.8	12	300	34.9	39.34
9	10	1.5	12	300	43.6	43.38
10	20	0.2	12	300	15.2	16.38
11	20	0.5	12	300	31.1	27.13
12	20	0.8	12	300	31.3	34.33
13	20	1.5	12	300	37.1	37.38
14	30	0.2	12	300	12.7	13.64
15	30	0.5	12	300	28.5	23.96
16	30	0.8	12	300	29.9	30.75
17	30	1.5	12	300	32.3	32.81
18	40	0.2	12	300	10.7	12.33
19	40	0.5	12	300	25.6	22.23
20	40	0.8	12	300	25.9	28.59
21	40	1.5	12	300	29.7	29.67
22	50	0.2	12	300	10.7	12.44
23	50	0.5	12	300	25.6	21.92
24	50	0.8	12	300	25.9	27.86
25	50	1.5	12	300	29.7	27.95
26	20	1	24	300	36	36.00
27	10	1	24	300	50.9	50.90
28	10	1	12	100	45.8	47.25
29	10	1	12	200	47.2	43.33
30	10	1	30	400	60.3174	60.32
31	10	1	12	500	50.4	49.92

P-value of 0.05, it is concluded that initial concentration dosage stirring speed and quadratic dosage are important terms. The plot of measured versus calculated values of removal (%) demonstrate a solid match (Figure 7) with R^2 of 0.967. This implies that 967% of the variations for percent removal are explained by the independent variables and the presence of a linear relationship between them with high correlation coefficient shows the normal distribution of error, the great applicability of model for clarification of exploratory information. These plots are required to check the ordinariness supposition in the fitted model. Adjusted R^2 is also a measure of goodness of a fit. Here, the Adj–R^2 value (0.946) was very close to the corresponding R^2 value.

Table 4 shows the regression results of the predicted response surface quadratic model for the ammonia removal by TiO_2/C_3N_4 in the form of ANOVA. ANOVA is required

Table 3 | Analysis of variance (ANOVA)

Source	DF	Adj SS	Adj MS	F-value	*P*-value
Model	12	4052.97	337.747	44.40	0.000
Linear	4	936.04	234.011	30.76	0.000
Initial concentration (ppm)	1	111.14	111.135	14.61	0.001
Dosage (g)	1	39.90	39.904	5.25	0.034
Light intensity	1	26.41	26.413	3.47	0.079
Stirring speed (rpm)	1	36.19	36.193	4.76	0.043
Square	4	605.98	151.496	19.91	0.000
Initial concentration (ppm)*Initial concentration (ppm)	1	32.07	32.073	4.22	0.055
Dosage (g)*Dosage (g)	1	329.16	329.162	43.27	0.000
Light intensity*Light intensity	1	22.94	22.938	3.02	0.100
Stirring speed (rpm)*Stirring speed (rpm)	1	48.95	48.951	6.43	0.021
2-Way interaction	4	93.23	23.307	3.06	0.043
Initial concentration (ppm)*Dosage (g)	1	18.61	18.609	2.45	0.135
Initial concentration (ppm)*Light intensity	1	42.57	42.573	5.60	0.029
Dosage (g)*Light intensity	1	23.23	23.226	3.05	0.098
Light intensity*Stirring speed (rpm)	1	31.53	31.529	4.14	0.057
Lack of fit	10	89.138	8.914	1.7497	0.254792
Error	18	136.94	7.608		
Total	30	4189.90			

S	R-sq	R-sq(adj)
2.75820	96.73%	94.55%

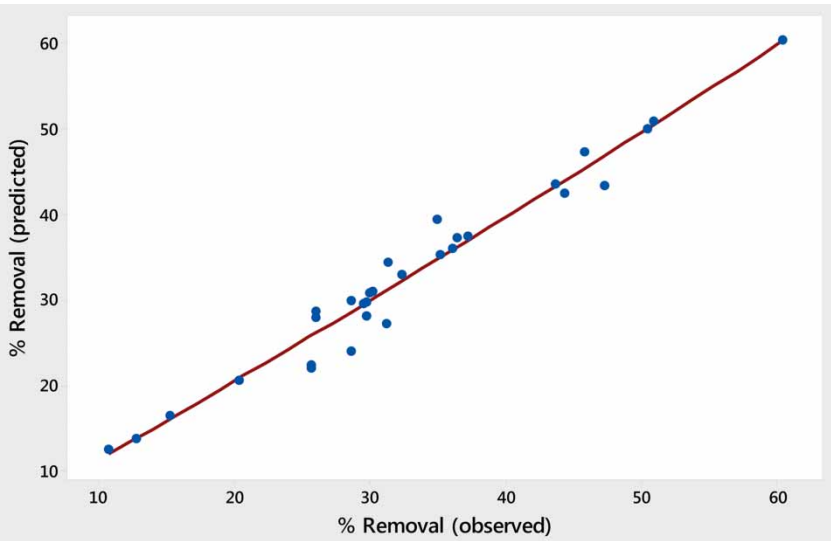

Figure 7 | The actual data versus predicted data for removal of ammonia.

Table 4 | Regression coefficients

Term	Coef	SE coef	T-value	*P*-value
Constant	26.28	3.23	8.13	0.000
Initial concentration (ppm)	−15.49	4.05	−3.82	0.001
Dosage (g)	40.3	17.6	2.29	0.034
Light intensity	−24.9	13.4	−1.86	0.079
Stirring speed (rpm)	17.77	8.15	2.18	0.043
Initial concentration (ppm)*Initial concentration (ppm)	2.85	1.39	2.05	0.055
Dosage (g)*Dosage (g)	−8.31	1.26	−6.58	0.000
Light intensity*Light intensity	−28.9	16.6	−1.74	0.100
Stirring speed (rpm)*Stirring speed (rpm)	6.12	2.41	2.54	0.021
Initial concentration (ppm)*Dosage (g)	−1.83	1.17	−1.56	0.135
Initial concentration (ppm)*Light intensity	−19.22	8.12	−2.37	0.029
Dosage (g)*Light intensity	61.4	35.1	1.75	0.098
Light intensity*Stirring speed (rpm)	32.9	16.2	2.04	0.057

to test the significance of the model. ANOVA is used to show whether the variation from the model is significant or not. This is performed by F-value. If the model is a good predictor of the experimental values, the F-value should be greater than the tabulated value of F at a level of significance α. The F-value obtained, 44.4, is clearly greater than the tabulated F (2.34 at 95% significance) confirming the adequacy of the model fits.

Photocatalytic degradation of ammonia

Effects of ammonia initial concentrations

Figure 8 demonstrates the impact of ammonia concentration on the removal percentage against time at constant stirring speed (300 rpm), time (50 min), light intensity (12 W), and dosage of catalyst (0.2 g/L).

It can be concluded that the degradation rate was high at the beginning of the photocatalytic reaction, and then it became low at the last 10 min. The rate of removal also decreases with the increasing concentration of ammonia in the simulated water. The removal at its initial concentration of 10 mg/L reached up to the maximum value of removal percentage.

From previous investigations, the reasons for this may be due to the fact that at lower ammonia concentration the photocatalytic oxidation was mainly governed by the adsorption of NH4 + on TiO_2/C_3N_4, any increase in initial concentration led to an increase in the amount of adsorption of ammonia. On the other hand, at very high concentrations the titanium dioxide surface becomes saturated owing to reaching adsorption/desorption equilibrium, and the photonic efficiency reduces, thus leading to catalyst deactivation.

Effect of catalyst dosage

The impact of the dosage of TiO_2/g-C_3N_4 composite on the photocatalytic degradation of ammonia was examined at a

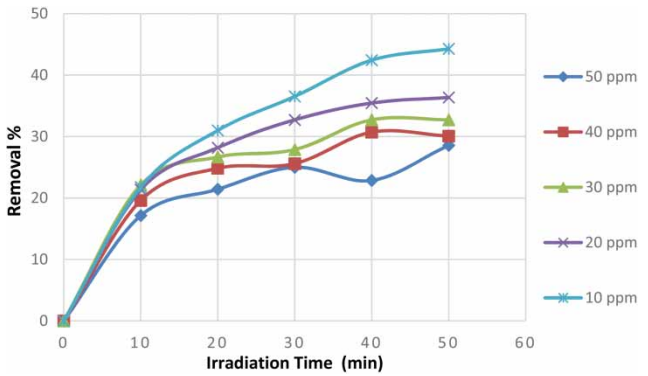

Figure 8 | Effect of ammonia initial concentration on the degradation of ammonia using TiO_2/C_3N_4 at stirring speed = 300 rpm, time = 50 min, light intensity = 12 W, and dosage of catalyst = 0.2 g/L.

constant stirring speed (300 rpm), time (50 min), light intensity (12 W), and concentration of 10 ppm. The results in Figure 9 show that the optimal dosage of TiO_2/g-C_3N_4 composite was found to be 1 g/L. A possible reason is that when the initial dosage of TiO_2/g-C_3N_4 composite powder is increased, the amount of involved photolysis reaction of TiO_2/g-C_3N_4 composite particles is increased, and the degradation rate is also increased. However, higher catalyst amounts make solid particles hinder the UV light, and light scattering increases (not enough light reaches the surface). Hence, the photo degradation efficiency is reduced (Altomare *et al.* 2014).

Effect of light intensity

As shown in Figure 10, by utilizing the optimum dosage and optimum ammonia initial concentration (at a constant stirring speed (300 rpm), time (50 min), catalyst dosage1 g/L, and concentration of 10 ppm), it was seen that while when increasing the light intensity a remarkable rate of removal is noticed, due to the huge increment of the light propagation across the reactor. The UV irradiation produces the photons required for the electron transfer from the valence band to the conduction band of a semiconductor photocatalyst, and the energy of the photon is dependent on the light intensity. Also, as more radiations fall on the catalyst surface and the rate of removal increases, the more hydroxyl radicals are produced. The enhancement of removal rate is due to an increase in hydroxyl radical concentration, hence the increase in the light intensity increases the removal (Nasser *et al.* 2009).

Effect of stirring speed on the percentage removal of ammonia

Changing the speed of mixing at time 50 min, catalyst dosage1 g/L, light intensity (12 W) and concentration of 10 ppm, an increase in the removal rate was observed as demonstrated in Figure 11. Photocatalysis is controlled by two steps, mass-transfer and chemical reaction. The mass transfer step is affected by the mixing speed. So, increasing of the mixing speed leads to a higher mass transfer and a high degradation rate. Also, increasing the mixing speed can promote oxygen transfer on the liquid phase (Merabet *et al.* 2009), which leads to an increase in the degradation rate.

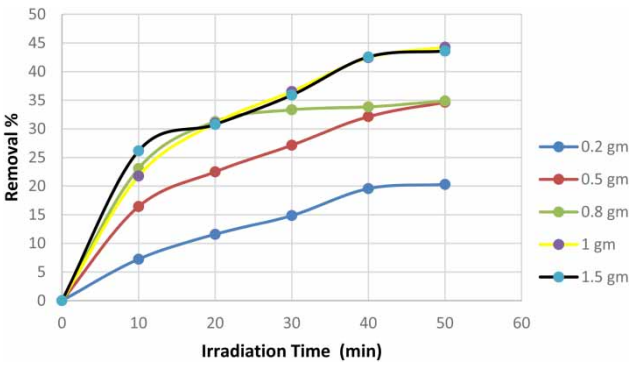

Figure 9 | Effect of catalyst dosage on degradation of ammonia at stirring speed = 300 rpm, time = 50 min, light intensity = 12 W, and concentration = 10 ppm.

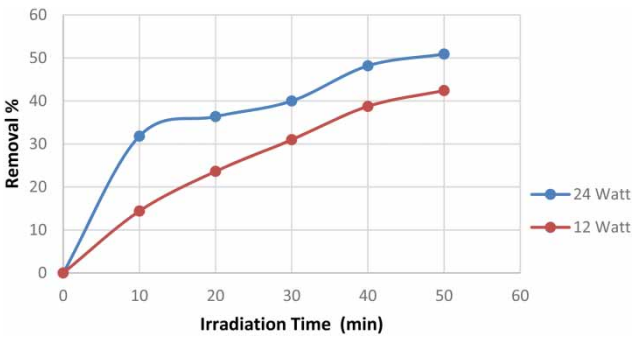

Figure 10 | Effect of light intensity on the degradation of ammonia using TiO_2/C_3N_4 at stirring speed = 300 rpm, time = 50 min, catalyst dosage = 1 g/L, and concentration = 10 ppm.

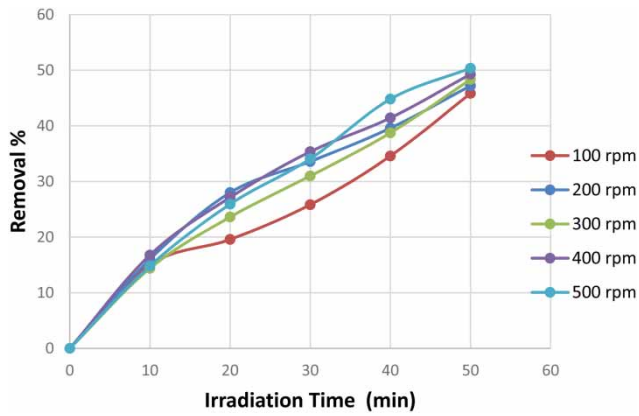

Figure 11 | Effect of stirring speed on the degradation of ammonia using TiO_2/C_3N_4 at light intensity = 12 W, time = 50 min, catalyst dosage = 1 g/L, and concentration = 10 ppm.

Comparison of photocatalytic activity of the two composites

To understand the efficiency of different composites, trials were carried out at fixed conditions of initial concentration, catalyst weight, light intensity and stirring speed. The efficiency of TiO_2/g-C_3N_4 and ZnO/g-C_3N_4 were examined and the results are presented in Figure 12. The results clearly indicate that ZnO/g-C_3N_4 was found to be the most active in the degradation of ammonia. This could be because the recombination of photo excited electrons in the large particles is slower than that in the small particles which concludes that the fast recombination in small particles occurred on the surface which led to an increase in the photocatalytic activity. Doping with ions and heterojunction coupling has been reported to enhance separation of the electron-hole pair and was found to reduce recombination and therefore enhance the interfacial charge transfer efficiency which leads to an improvement in the photocatalytic activity (Pelaez *et al.* 2012).

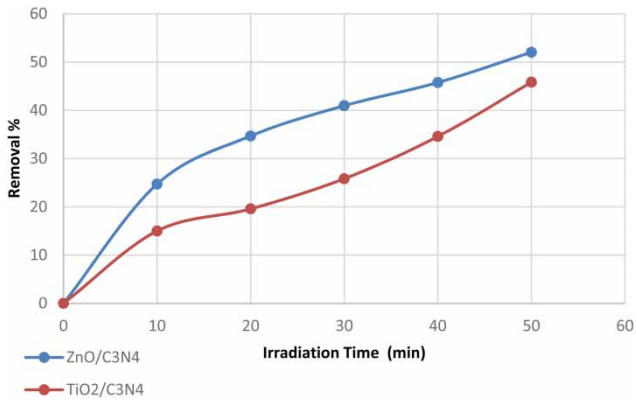

Figure 12 | Comparison of efficiency of TiO_2/C_3N_4 and ZnO/C_3N_4 composites on the degradation of ammonia at stirring speed = 300 rpm, time = 50 min, catalyst dosage = 1 g/L, light intensity = 12 W and concentration = 10 ppm.

Response surface methodology

The three-dimensional response surface plots give well-recognized knowledge about the main effect of four variables (Figure 13). To study the impact of the initial concentration on the removal efficiency, some experiments with 0.2–1.5 g of adsorbent at light intensity ranging from 6 to 30 W with a stirring speed ranging from 100 to 500 rpm were designed. The results in Figure 13(a) indicate that raising the catalyst dosage causes a significant improvement in the removal efficiency which emerged from an increase in available surface and the presence of active surface area of the catalyst surfaces that enables ammonia adsorption. However, increasing ammonia initial concentration is joined by a decrease in the removal efficiency. To concentrate the effect of the initial concentration on the adsorption efficiency, a few runs with concentrations of 10–50 mg L^{-1} adsorbent at a light intensity of 12 W and stirring speed of 100–500 rpm were designed and the results are displayed in Figure 13(b).

The noticed decreases in removal percentage at higher initial concentrations arise from the lower ratio of vacant sites on catalyst for ammonia molecules that are competing for binding to the surface. This means that there are not enough sites for all molecules in high ammonia concentrations. As shown in Figure 13(c), the more catalyst quantity associated with high adsorption efficiency and increased stirring speed leads to better and higher removal efficiency.

CONCLUSIONS

Different photocatalysts (ZnO/g-C_3N_4, TiO_2/g-C_3N_4) were prepared using different precursors. The composites were

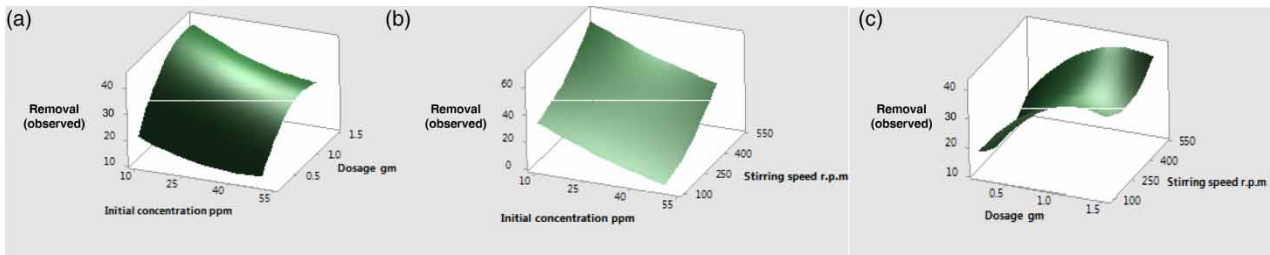

Figure 13 | Response surfaces for the ammonia removal: (a) initial concentration–dosage; (b) initial concentration–stirring speed; (c) dosage–stirring speed.

characterized by Fourier transform infrared spectroscopy (FTIR), scanning electron microscope (SEM) and X-ray powder diffraction (XRD). Their efficiency was researched by the degradation of an ammonia solution. The use of RSM based on CCD was applied for optimization of parameters such as initial concentration, catalyst dosage, light intensity and stirring speed. The results indicate that the photocatalytic degradation of the ammonia solution, after 50 min of UV irradiation, can reach percentages of 46%, and 52% using the catalysts TiO_2/g-C_3N_4 and ZnO/g-C_3N_4, respectively, which suggests that ZnO/g-C_3N_4 has a higher degradation efficiency.

ACKNOWLEDGEMENTS

This work was financially supported by the Petrochemical Engineering Department, Pharos University, Alexandria, Egypt.

REFERENCES

Achouri, F., Corbel, S., Aboulaich, A., Balan, L., Ghrabi, A., Said, M. B. & Schneider, R. 2014 Aqueous synthesis and enhanced photocatalytic activity of ZnO/Fe_2O_3 heterostructures. *J. Phys. Chem. Solids* **75** (10), 1081–1186.

Akarsu, M., Asiltürk, M., Sayilkan, F., Kiraz, N., Arpac, E. & Sayilkan, H. 2006 A novel approach to the hydrothermal synthesis of anatase titania nanoparticles and the photocatalytic degradation of rhodamine B. *Turk. J. Chem.* **30**, 333–343.

Altomare, M., Dozzia, M. V., Chiarelloa, G. L., Paolab, A. D., Palmisanob, L. & Selli, E. 2014 High activity of brookite TiO_2 nanoparticles in the photocatalytic abatement of ammonia in water. *Catal. Today* **252**, 184–189.

Alwan, R. M., Kadhim, Q. A., Sahan, K. M., Ali, R. A., Mahdi, R. J., Kassim, N. A. & Jassim, A. N. 2015 Synthesis of zinc oxide nanoparticles via sol–gel route and their characterization. *Nanosci. Nanotechnol.* **5** (1), 1–6.

Amano, F., Ishinaga, E. & Yamakata, A. 2013 Effect of particle size on the photocatalytic activity of WO_3 particles for water oxidation. *J. Phys. Chem. C* **117** (44), 22584–22590.

Bali, U. 2004 Application of Box–Wilson experimental design method for the photodegradation of textile dyestuff with UV/ H_2O_2 process. *Dyes Pigm.* **60**, 187–195.

Dong, S. S., Zhang, J. B., Gao, L. L., Wang, Y. L. & Zhou, D. D. 2012 Preparation of spherical activated carbon supported and Er^{3+}:$YAlO_3$ doped TiO_2 photocatalyst for methyl orange degradation under visible light. *Trans. Nonferrous Met. Soc. China* **22**, 2477–2483.

Gupta, V. K., Sadegh, H., Yari, M., Ghoshekandi, R. S., Maazinejad, B. & Chahardori, M. 2015 Removal of ammonium ions from wastewater: a short review in development of efficient method. *Glob. J. Environ. Sci. Manage.* **1** (2), 149–158.

Jiang, H. B., Cuan, Q., Wen, C. Z., Xing, J., Wu, D., Gong, X.-Q., Li, C. & Yang, H. G. 2011 Anatase TiO_2 crystals with exposed high-index facets. *Angew. Chem. Int. Edn.* **50** (16), 3764–3768.

Jiangyan, W., Jinliang, Y., Wei, Y. & Ting, L. 2012 Structural and optical properties of Zn_3N_2 films prepared by magnetron sputtering in NH_3–Ar mixture gases. *J. Semicond.* **33** (4), 043001.

Komatsu, T. 2001a Attempted chemical synthesis of graphite-like carbon nitride. *J. Mater. Chem.* **11**, 799–802.

Komatsu, T. 2001b Prototype carbon nitrides similar to the symmetric triangular form of melon. *J. Mater. Chem.* **11**, 802–805.

Komatsu, T. 2001c The first synthesis and characterization of cyameluric high polymers. *Macromol. Chem. Phys.* **202**, 19–25.

Li, X. F., Zhang, J. & Shen, L. H. 2009 Preparation and characterization of graphitic carbon nitride through pyrolysis of melamine. *Appl. Phys. A Mater. Sci. Proc.* **94**, 387–392.

Luo, X., Yan, Q., Wang, C., Luo, C., Zhou, N. & Jian, C. 2015 Treatment of ammonia nitrogen wastewater in low concentration by two-stage ozonization. *Int. J. Environ. Res.* **12** (9), 11975–11987.

Merabet, S., Bouzaza, A. & Wolbert, D. 2009 Photocatalytic degradation of indole in a circulating upflow reactor by UV/TiO_2 process – influence of some operating parameters. *J. Hazard. Mater.* **166**, 1244–1249.

Mikami, I., Aoki, S. & Miura, Y. 2010 Photocatalytic oxidation of aqueous ammonia in the presence of oxygen over platinum-loaded TiO_2. *Chem. Lett.* **39** (l), 704–705.

Miranda, C., Mansilla, H., Yánez, J., Obregón, S. & Colón, G. 2013 Improved photocatalytic activity of g-C_3N_4/TiO_2 composites prepared by a simple impregnation method. *J. Photochem. Photobiol. A Chem.* **253**, 16–21.

Nasser, M., Behnajady, A. M., Oskui, J. & Reza, M. 2009 Investigation of the efficiency of ZnO photocatalyst in the removal of p-nitrophenol from contaminated water, Iran. *J. Chem. Chem. Eng.* **28** (1), 49–55.

Oliveira, R., Almedia, M. F., Santos, L. & Madeira, L. M. 2006 Experimental design of 2,4-dichlorophenol oxidation by Fenton's reaction. *Ind. Eng. Chem. Res.* **45**, 1266–1276.

Pelaez, M., Nolan, N. T., Pillai, S. C., Seery, M. K., Falaras, P., Kontos, A. G. & Entezari, M. H. 2012 A review on the visible light active titanium dioxide photocatalysts for environmental applications. *Appl. Catal. B* **125**, 331–349.

Salavati-Niasari, M., Hosseinzadeh, G. & Davar, D. 2011 Synthesis of lanthanum carbonate nanoparticles via sonochemical method for preparation of lanthanum hydroxide and

lanthanum oxide nanoparticles. *J. Alloys Comp.* **509** (1), 134–140.

Shavisi, Y., Sharifnia, S., Hosseini, S. N. & Khadivi, M. A. 2013 Application of TiO_2/perlite photocatalysis for degradation of ammonia in wastewater. *J. Ind. Eng. Chem.* **20** (1), 278–283.

Xiong, H.-M., Shchukin, D. G., Möhwald, H. X. Y. & Xia, Y. Y. 2009 Sonochemical synthesis of highly luminescent zinc oxide nanoparticles doped with magnesium (II). *Angew. Chem. Int. Edit.* **48**, 2727–2731.

Yuzawa, H., Mori, T., Itoh, H. & Yoshida, H. 2012 Reaction mechanism of ammonia decomposition to nitrogen and hydrogen over metal loaded titanium oxide photocatalyst. *J. Phys. Chem. C* **116**, 4126–4136.

Zhou, Y., Xiao, B., Liu, S.-Q., Meng, Z., Chen, Z.-G., Zou, C.-Y., Liu, C.-B., Chen, F. & Zhou, X. 2016 Photo-Fenton degradation of ammonia via a manganese–iron double-active component catalyst of graphene–manganese ferrite under visible light. *Chem. Eng. J.* **283**, 266–275.

First received 29 July 2017; accepted in revised form 27 November 2017. Available online 4 January 2018